(Received 15 December 2025, Accepted 6 January 2026, Scheduled 6 February 2026)

A Parallel Block Splitting FFT Method for Efficient Computation of Electromagnetic Scattering from Time-Varying Sea Surface

Zhiwei Liu, Feng Xia*, Rui Wang, and Xiaoyan Zhang

School of Information and Software Engineering, East China Jiaotong University, Nanchang 330000, China

ABSTRACT: 2-D Fast Fourier transform (FFT) is the most time-consuming step for the modeling of time-varying sea surface using high-order small slope approximation (SSA). In this paper, a parallel block splitting method is proposed to accelerate 2D FFT calculation. The whole 2-D FFT matrix is divided into $m \times n$ blocks, and the traditional 2-D FFT is applied to each block in parallel. Finally, the complete FFT result can be obtained by using the message passing interface (MPI) for data communication and superimposing phase factors. This method can effectively reduce the communication overhead by combining symmetric domain decomposition and is more suitable than traditional parallel libraries. Accordingly, both generations of the sea surface and computation of scattering using SSA can be accelerated. Numerical experiments demonstrate that the proposed method exhibits strong scalability. Under a four-node configuration, the parallel efficiency of sea surface generation reaches 61.2%, while the second-order SSA parallel efficiency achieves 80.7%. This effectively resolves low-efficiency issues in large-scale sea surface generation and serial SSA computations.

1. INTRODUCTION

With the rapid development of marine environmental research and defense needs, the rapid generation of time-varying sea surfaces and the fast calculation of sea surface electromagnetic scattering have garnered significant attention [1, 2]. How to fully utilize computer resources to rapidly simulate and calculate the electromagnetic scattering characteristics of vast sea surfaces has become a current research hotspot.

The methods for generating sea surfaces are primarily categorized into linear superposition method and linear filtering method. The former treats sea waves as a linear superposition of a series of harmonic waves with varying amplitudes, frequencies, phases, and directions. However, this method cannot accurately simulate the nonlinear characteristics of real-world sea waves, such as wave crest sharpening, wave trough flattening, and wave breaking. The latter utilizes the Fast Fourier Transform (FFT) to simulate the undulation characteristics of large-scale sea surfaces under different wind speeds and directions. It has the prominent advantages of high computational efficiency, fast speed, and more distinct sea surface features, and is widely applied to the field of sea surface electromagnetic scattering calculation.

The common methods of sea surface electromagnetic scattering calculation can be broadly categorized into two types: numerical methods and approximate methods. Numerical methods, such as the Method of Moments (MoM) [3], Finite-Difference Time-Domain (FDTD) method [4], and Forward-Backward Iterative Method (FBM) [5], have been widely applied in electromagnetic scattering research. Numerical methods offer high computational accuracy but suffer from drawbacks, such as fine mesh partitioning, massive memory requirements, and lengthy iteration times, and their accuracy is dependent on the mesh structure, making them unsuitable for electromagnetic scattering applications involving electrically large or ultra-large sea surfaces. Commonly used approximate methods include the perturbation method (SPM) [6], Kirchhoff plane approximation method (KA) [7], and small slope approximation method (SSA) [8]. The approximation method is subject to model constraints, such as incident wavelength, height variance of rough surfaces, correlation length, and root mean square slope. SSA is applied to electromagnetic waves of any wavelength and for surfaces with small inclination angles, and it is a relatively accurate approximation method. Different orders of approximation yield different results. Under certain conditions, they can degenerate into perturbation methods and Kirchhoff approximations. Second-order SSA has been proven to have good computational accuracy [9], but its computational complexity reaches $O(N^2)$, resulting in high computational complexity. For example, due to the high computational complexity of second-order SSA, some researchers have proposed a simplified formula for backscattering to reduce computational workload [10].

With the development of computer technology, the demand for rapid generation and scattering calculation of large-scale and ultra-large-scale time-varying sea surface gradually appears, and FFT technology, which restricts the core performance of the algorithm, has attracted attention. Several FFT fast calculation algorithm libraries based on CPUs or GPUs have been developed, such as FFT in the west (FFTW) [11] and Math Kernel Library (MKL) [12] for CPUs, and CUDA FFT (cuFFT) [13] and OpenCL FFT (clFFT) [14] for GPUs. Among them, FFTW is a serial C program, an adaptive soft-

* Corresponding author: Feng Xia (xfvxh2599@163.com).

ware package developed by the Supercomputing Group at the Computer Science Laboratory of the Massachusetts Institute of Technology, which is recognized as the fastest and most widely used software package in the world. In distributed computing, the main problem is communication overhead. Koopman and Bisseling [15] proposed to reduce communication overhead by limiting global communication to a single All-to-All operation through specific data decomposition in multi-dimensional FFT. Cayrols et al. [16] compressed the frequency domain data before MPI transmission, thus directly reducing the amount of data transmitted by the network.

However, the first-order SSA only needs to consider the primary scattering effect on the rough surface of electromagnetic waves, and the second-order SSA needs to consider the multiple scattering effect on the rough surface, so the current parallel research is mainly used for the first-order SSA calculation. For example, the MPI parallel method proposed by Wang et al. [17] is for the first-order SSA, and the GPU parallel method proposed by Jiang et al. [18] is also for the first-order SSA, while the second-order SSA is not applicable. Second-order SSA has a large amount of calculation and needs to store a large amount of data, which makes the existence of a super-large sea surface in a single machine unbearable and requires regional decomposition. However, if the mainstream FFT parallel library is directly used after domain decomposition, it will lead to serious communication overhead and seriously reduce parallel efficiency.

Therefore, based on the above problems, in order to solve the problem of large single-machine memory demand, this paper uses MPI + symmetrical domain decomposition to slow down the memory pressure. In order to solve the problem of incompatibility of the general FFT parallel library, a block FFT parallel method is proposed to reduce communication overhead. Finally, in order to further accelerate the second-order SSA, the integral calculation is accelerated by combining OpenMP.

2. PHASE COMPENSATION PRINCIPLE OF BLOCK FFT METHOD

Because of the superior performance of the FFTW library, this paper makes use of parallelism on the basis of this library. First, the matrix requiring FFT is decomposed into matrix blocks with the same size according to the number of nodes and assigned to each node. Each node completes a two-dimensional FFT and then aggregates to the master node for phase compensation. In order to facilitate the understanding of the principle of block FFT splitting and phase compensation, this paper will extend from one dimension to two dimensions.

2.1. Principle of One-Dimensional FFT Chunking

First, let's discuss the one-dimensional block method of FFT. Suppose that there is a discrete sequence $\{x_n\} = \{x, x_1, \ldots, x_{N-1}\}$ that needs to be divided into k parts. First, N must be a multiple of k. Performing a discrete Fourier transform on it will yield $\{X_m\} = \{X, X_1, \ldots, X_{N-1}\}$. Then,

$$X_m = \sum_{n=0}^{N-1} x_n e^{-j2\pi m \frac{n}{N}}. \tag{1}$$

where $m = 0, 1, \ldots, N-1$. Here, N is a multiple of k. The calculation process of Equation (1) is divided into k parts according to the modulo k congruence of the x_n.

$$\begin{aligned} X_m &= \sum_{r=0}^{k-1} \sum_{n=0}^{\frac{N}{k}-1} x_{kn+r} e^{-j2\pi m \frac{kn+r}{N}} \\ &= \sum_{r=0}^{k-1} e^{-j2\pi rm/N} \sum_{n=0}^{\frac{N}{k}-1} x_{kn+r} e^{-j2\pi mn/\frac{N}{k}} \end{aligned} \tag{2}$$

In the formula, the r term can be regarded as the Fourier transform of the sequence $\{x_{kn+r}\}$, where $r = 0, 1, \ldots, N/k-1$, $n = 0, 1, \ldots, N-1$. Let

$$X_m^r = \sum_{n=0}^{\frac{N}{k}-1} x_{kn+r} e^{-j2\pi mn/\frac{N}{k}}, \tag{3}$$

Since the sequence length is reduced to $1/k$ of the original, when $\{X_{rN/k}, X_{rN/k+1}, \ldots, X_{(r+1)N/k-1}\}$ is calculated, the Fourier transform expression can be written as

$$\begin{aligned} X_{m+\frac{rN}{k}} &= \sum_{s=0}^{k-1} e^{-j2\pi s\left(m+\frac{rN}{k}\right)/N} X^s_{m+\frac{rN}{k}} \\ &= \sum_{s=0}^{k-1} e^{-j2\pi \frac{sr}{k}} e^{-j2\pi sm/N} X_m^s \end{aligned} \tag{4}$$

The above is the principle of one-dimensional block partitioning of k, wherein N is the sequence length; n is the n-th element in the sequence; m is the m-th element in the sequence after the Fourier transform; k is the number of blocks of the sequence; r is the r-th sequence after blocking. For one-dimensional sequences, phase loss or phase splitting occurs when the FFT is completed in each sub-block sequence X_m. It is necessary to calculate and then compensate for the two-phase factors according to Equation (4), which is the one-dimensional FFT phase compensation operation.

2.2. Principle of Two-Dimensional FFT Chunking

Suppose that there is a set of two-dimensional discrete sequences $\{x_{mn}\} = \{x_0, x_{0,1}, \ldots, x_{M-1,N-1}\}$, where M and N are multiples of k and l, respectively. Performing a two-dimensional discrete Fourier transform on this set yields $\{X_{pq}\} = \{X_0, X_{0,1}, \ldots, X_{M-1,N-1}\}$, then

$$X_{p,q} = \sum_{m=0}^{M-1} \sum_{n=0}^{N-1} x_{m,n} e^{-j2\pi \frac{pm}{M}} e^{-j2\pi \frac{qn}{N}}. \tag{5}$$

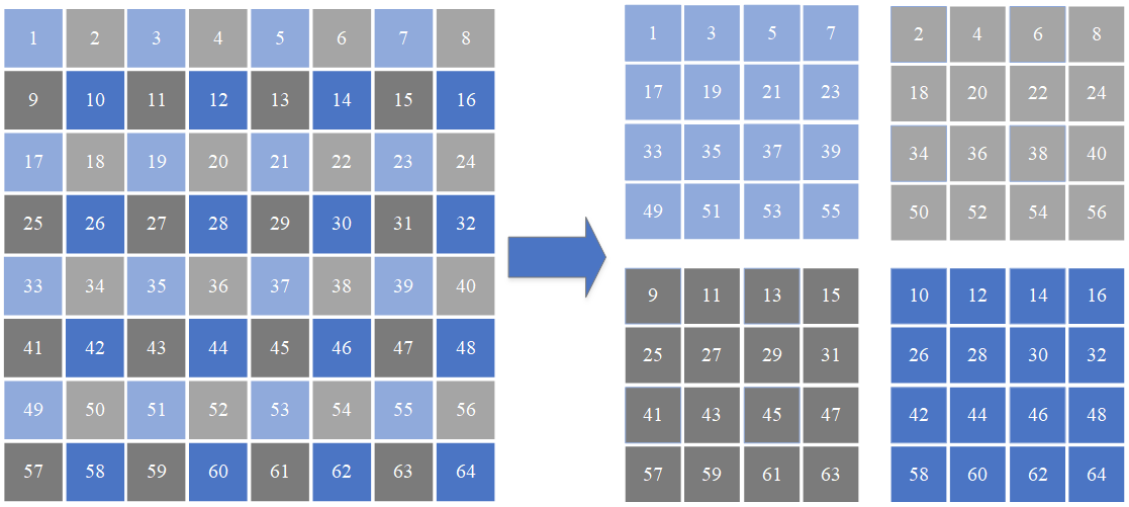

FIGURE 1. Schematic diagram of 4-node matrix splitting.

where $p = 0, 1, \ldots, M-1$, $q = 0, 1, \ldots, N-1$. Since M is a multiple of k, and N is a multiple of l, the Fourier transform can be decomposed into

$$X_{p,q} = \sum_{r=0}^{\frac{M}{k}-1} \sum_{s=0}^{\frac{N}{l}-1} \sum_{m=0}^{\frac{M}{k}-1} \sum_{n=0}^{\frac{N}{l}-1} x_{km+r,ln+s} e^{-j2\pi p(km+r)/M} e^{-j2\pi q(ln+s)/N}, \tag{6}$$

Due to

$$X_{p,q}^{r,s} = \sum_{m=0}^{\frac{M}{k}-1} \sum_{n=0}^{\frac{N}{l}-1} x_{km+r,ln+s} e^{-j2\pi pm/\frac{M}{k}} e^{-j2\pi qn/\frac{N}{l}}, \tag{7}$$

it can be expressed as the two-dimensional Fourier transform of the data block in row r and column s. Therefore, the two-dimensional Fourier transform of $\{x_0, x_{0,1}, \ldots, x_{M/k-1,N/l-1}\}$ can be expressed as

$$X_{p,q} = \sum_{r=0}^{\frac{M}{k}-1} \sum_{s=0}^{\frac{N}{l}-1} e^{-j2\pi pr/M} e^{-j2\pi qs/N} X_{p,q}^{r,s}. \tag{8}$$

The two-dimensional Fourier transform of $\{x_{rM/ksN/l}, \ldots, x_{(r+1)M/k-1,(s+1)N/l-1}\}$ can be expressed as

$$\begin{aligned} & X_{p+\frac{rM}{k},q+\frac{sN}{l}} \\ &= \sum_{r=0}^{\frac{M}{k}-1} \sum_{s=0}^{\frac{N}{l}-1} e^{-j2\pi\left(p+\frac{rM}{k}\right)r/M} e^{-j2\pi\left(q+\frac{sN}{l}\right)s/N} X_{p+\frac{rM}{k},q+\frac{sN}{l}}^{r,s} \\ &= \sum_{r=0}^{\frac{M}{k}-1} \sum_{s=0}^{\frac{N}{l}-1} e^{-j2\pi\frac{r^2}{k}} e^{-j2\pi\frac{s^2}{l}} e^{-j2\pi\frac{pr}{M}} e^{-j2\pi\frac{qs}{N}} X_{p,q}^{r,s}. \end{aligned} \tag{9}$$

The above is the principle of two-dimensional partitioning. Among them, M and N are the sizes of matrix rows and columns, respectively; m and n are the matrix rows and columns; p and q are the rows and columns of the matrix after the Fourier transform; k and l are the numbers of row and column partitions; r and s are the row and column values after blocking. For a two-dimensional matrix, when the FFT is completed in each submatrix $X_{p,q}$, phase loss occurs, that is, phase splitting. It is necessary to calculate and then compensate for the four phase factors according to Equation (9), which is the two-dimensional FFT phase compensation operation.

2.3. Parallel Strategies for Block FFT Methods

In this paper, four nodes are taken as examples, and the matrix is divided into four small matrices according to the parity of rows and columns, and the splitting rule of Equation (6). As shown in Figure 1, an 8×8 matrix is split into four 4×4 small matrices, and each small matrix is assigned to each node to complete the FFT operation independently. Finally, the four small matrices after the FFT operation are aggregated into one node for phase compensation through Equation (9).

Firstly, the performance of the proposed method is analyzed theoretically. Taking a two-dimensional complex matrix of size $N_x \times N_y$ as an example, the complexity of the traditional two-dimensional FFT method is $O(N^2 \log N)$. If it is divided into $M \times M$ sub-matrices to perform block FFT calculations, respectively, the computational complexity of each submatrix can be reduced to $O(N^2 \log(N/M))$. In addition, block processing implements the parallel computation of the FFT algorithm. However, this method requires phase compensation at the end, which introduces additional computational overhead and reduces efficiency. However, this method implements block parallel computation of FFT, thus improving the overall parallel efficiency of the program. At the same time, in order to divide the number of blocks evenly, a small amount of continuation will be performed according to the number of nodes when the sea surface is generated.

3. APPLICATION OF THE BLOCK FFT METHOD IN THE CALCULATION OF ELECTROMAGNETIC SCATTERING AT SEA SURFACE

In this paper, the linear filtering method is used to generate the sea surface in real time. At time t, the height value at linear sea surface $r(x, y)$ can be obtained by the standard spectral method, that is

$$h(r,t) = \frac{1}{L_x L_y} \sum\sum A_L(k,t) \exp(j\mathbf{k}\cdot\mathbf{r}), \tag{10}$$

Among them

$$\begin{aligned} A_L(k,t) =& G(k)\pi \cdot \sqrt{2L_x L_y W(k,\phi) e^{j\omega(k)t}} \\ &+ G^*(-k)\pi \cdot \sqrt{2L_x L_y W(k,\pi-\phi) e^{-j\omega(k)t}}. \end{aligned} \tag{11}$$

where $G(k)$ is a two-dimensional random sequence, which conforms to a complex Gaussian distribution with zero mean and 1 variance; $G*(-k)$ is the reverse-order conjugate of $G(k)$; L_x and L_y are the lengths of two-dimensional sea surface in x-axis direction and y-axis direction, respectively; spatial wavenumber is $k = \sqrt{k_x^2 + k_y^2}$, whose propagation frequency and spatial wavenumber satisfy the dispersion relationship:

$$\omega(k) = \sqrt{g_0 |k| \left[1 + (k/k_m)^2\right]}. \tag{12}$$

Among them, g is the gravitational acceleration; k_m is related to the surface tension T and density ρ of seawater, and can be expressed as $k_m = (\rho g_0/T)^{1/2}$. In this paper, k_m is taken as 363.2 rad/m.

For a two-dimensional rough surface $z = h(r)$, the scattering amplitude expression for the second-order SSA is

$$\begin{aligned} & S_2(k_s, k_0) \\ =& \frac{1}{(2\pi)^2} \frac{2\left(q_1 q_{01}\right)^{1/2}}{\sqrt{P_{\text{inc}}}\left(q_{01}+q_1\right)} \int T[r, h(r)] \\ & \exp\left[-j(k_s - k_0)\cdot r + j(q_{01}+q_1)h(r)\right] \mathrm{d}r \\ & \times \left[B_1(k_s,k_0) - \frac{j}{4}\int M(k_s,k_0,\xi) h(\xi) \exp(j\xi\cdot r)\mathrm{d}\xi\right], \end{aligned} \tag{13}$$

Among them:

$$\begin{aligned} M(k_s,k_0,\xi) =& B_2(k_s,k_0,k_s-\xi) + B_2(k_s,k_0,k_0+\xi) \\ &+ 2(q_1+q_{01})B_1(k_s,k_0). \end{aligned} \tag{14}$$

where r is the projection of the spatial position vector R on the x-y plane; k_0 and q_{01} are the horizontal and vertical projection components of the incident wave in the air, respectively; k_s and q_1 are the horizontal and vertical projection components of scattered waves in the air, respectively; $h(\xi)$ is the Fourier transform of sea surface height; M matrix is the multiple-scattering term; $B_1(k_s, k)$ and $B_2(k_s, k, k+\xi)$ are first-order and second-order polarization factors, which are derived from the derivation of SPM coefficients and represent the influence of Bragg scattering on the results. The specific expressions can be found in [19].

Then, a statistically significant analytical expression is used to obtain the normalized radar cross section (NRCS), defined as

$$\Delta S(k_s,k_0) = S(k_s,k_0) - \langle S(k_s,k_0)\rangle, \tag{15}$$

Among them, $\langle\cdot\rangle$ denotes the set average, and * denotes the conjugation. Therefore, the second-order SSA normalized radar cross section can be expressed as

$$\sigma = 4\pi q_0 q_k \langle \Delta S(k_s,k_0) \times \Delta S^*(k_s,k_0)\rangle. \tag{16}$$

For the second-order SSA, the computational complexity reaches $O(N^2)$. Although applying the Fourier transform to the integral term M in Equation (13) can achieve acceleration, the parallelism of SSA will be broken by using the Fourier transform. In order to consider the general-purpose type, the common FFT parallel library generally needs to ensure that the master node has complete data and then perform FFT, which leads to serious communication overhead in the case of domain decomposition. To solve this problem, parallelism can be achieved by using domain decomposition for the sea surface and block FFT splitting for the FFT.

At the same time, since the FFT-shift operation is required after FFT, and the essence of two-dimensional FFT shift is double circulant permutation, in order to avoid the communication overhead caused by FFT shift, symmetrical domain decomposition can be used, as shown in Figure 2, which can avoid communication between nodes. As shown in Figure 2, taking the 8×8 sea surface divided into four nodes as an example, the intermediate axis of the horizontal axis of the matrix is the symmetry axis, and the sea surface is decomposed into symmetrical areas for each node to complete the operation independently.

When FFT calculations are required in the computation, each node is divided into the matrix shown in Figure 3 according to the rules in Equation (6) to perform independent FFT calculations, and only the necessary data needs to be distributed during each communication. For a complex matrix of $M*N$ size, if the FFTW parallel library is used, one distribution and one result aggregation are required. During FFT calculation, the strategy of the FFTW library is to perform one-dimensional FFT first, then transpose, and then perform one-dimensional FFT to realize two-dimensional FFT calculation, and one communication is also required during matrix transposition. Therefore, the traditional parallel library needs three complete data communications under the strategy of domain decomposition, that is, $24M * N$ bytes of communication. The block FFT splitting method only needs to send the required data when distributing data (as shown in Figure 3), send 3/4 of the data volume when distributing, and one complete data set when recovering, totaling $14M * N$ bytes of data, which can effectively reduce the fixed communication overhead, while the FFT calculation overhead remains consistent.

When the FFT operation is finished, it needs to be aggregated to one node for phase compensation, and finally distributed to

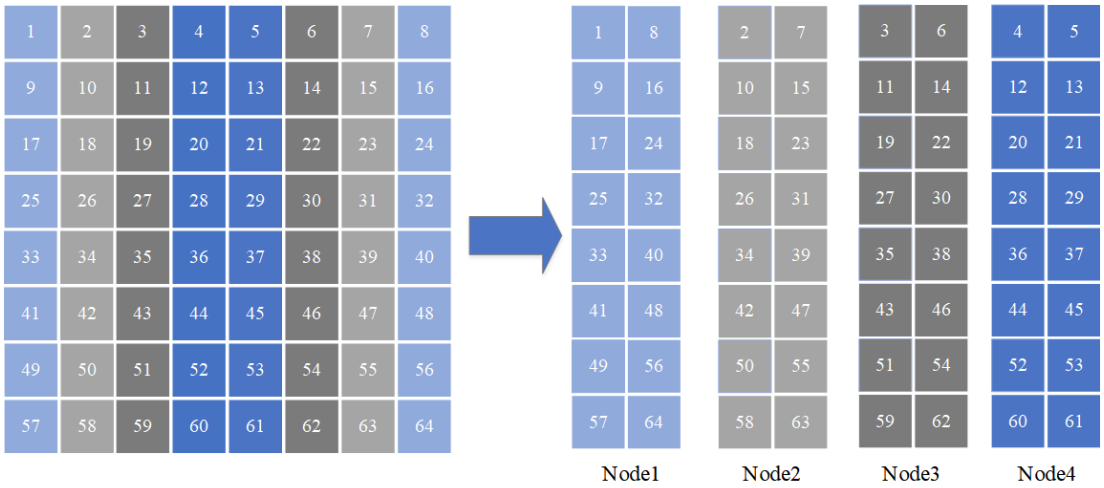

FIGURE 2. Schematic diagram of symmetric domain decomposition.

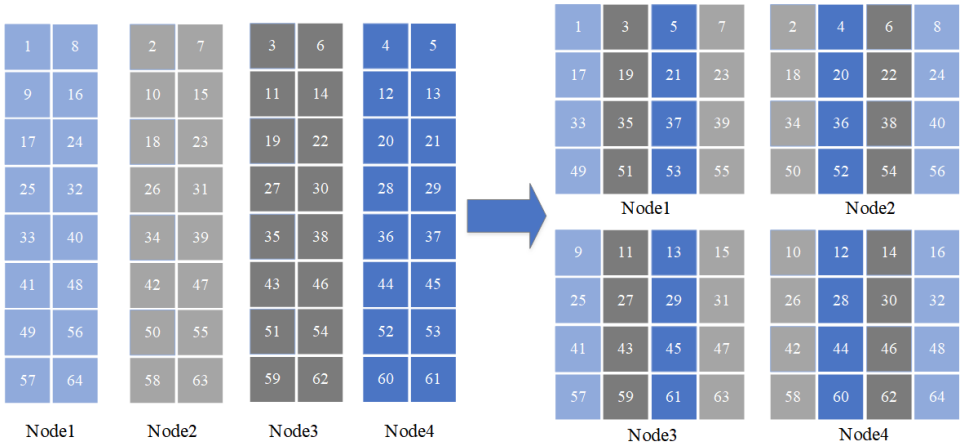

FIGURE 3. FFT data distribution diagram.

each node for the next operation according to the symmetric decomposition rule in Figure 2.

Therefore, the sea surface generation process of the block FFT parallel algorithm based on symmetric domain decomposition is as follows:

1. According to the splitting rule in Figure 2, the task is distributed to each node to complete the superposition of the sea spectrum and white noise in each region.

2. Distribute the obtained sea spectrum frequency domain signal matrix to each node according to the rule of Figure 3.

3. Each node independently completes the inverse Fourier transform calculation of some regions.

4. The complete sea surface height $h(r)$ is obtained by converging the calculation results of each node into the four phase factors in the main node compensation formula (9).

Since the second-order SSA needs FFT integration operation on the M matrix and FFT-shift operation, the FFT parallel strategy of sea surface generation and second-order SSA is consistent with the above strategy, and symmetric domain decomposition is still adopted. When the sea surface is generated, the parallel strategy of the second-order SSA is shown in Figure 4, and the calculation process of each node is consistent with that of Node2. Communication is performed only during the block FFT calculation. At the same time, in order to further accelerate the calculation, it is considered to introduce OpenMP to further accelerate the calculation when solving the M matrix and S matrix. After the calculation, the scattering amplitude S is recovered to calculate NRCS.

Due to the regional decomposition of the sea surface, the tapered wave also needs to be divided according to the division method of the sea surface area. That is, the electromagnetic wave irradiating each sub-area of the sea surface belongs to a part of the tapered wave that can cover the whole sea surface, and it is a complete cone wave after splicing. The detailed derivation method can be found in [20]. In this way, the scattering field of the whole sea surface can be obtained only by calculating the scattering field of each sub-region of the sea surface separately, and the final result is consistent with that directly calculated by formula (13).

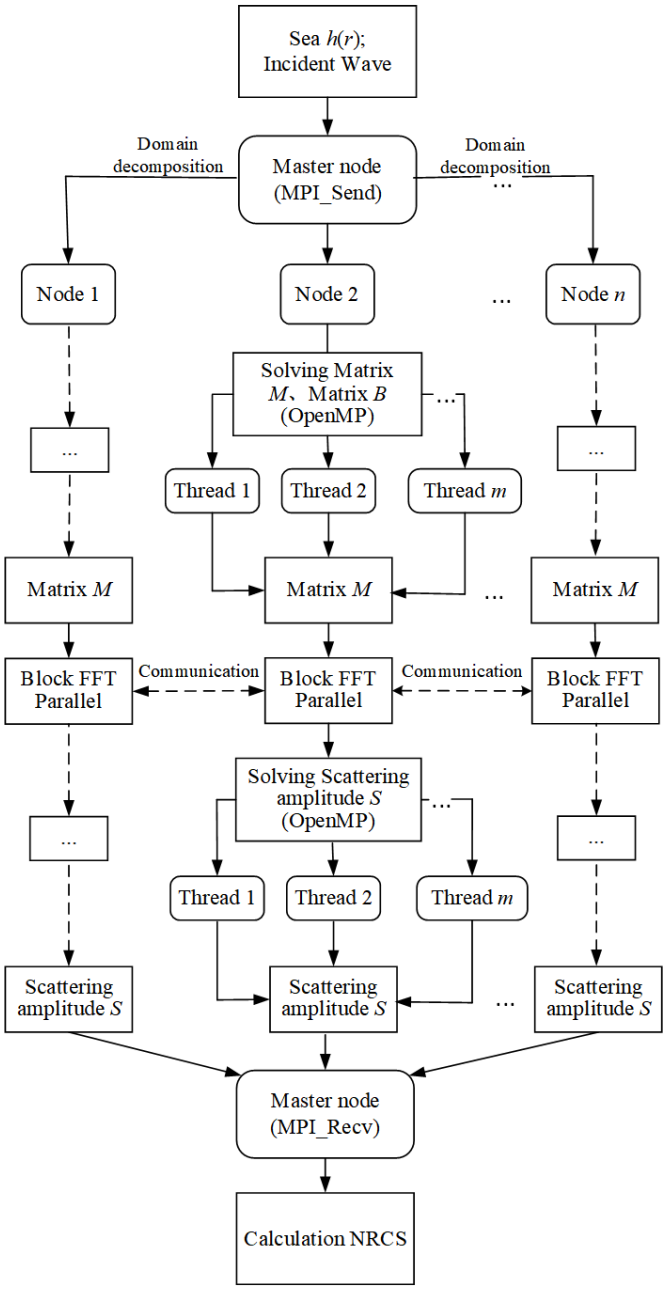

FIGURE 4. Second-order SSA parallel flowchart.

4. NUMERICAL RESULTS

Numerical experiments were conducted on Intel Core desktop Xeon E312xx (16-core) processors with 32 GB of memory per node and Windows 10 as the operating system; the MPI environment uses MPICH2.

4.1. Numerical Performance Testing of Block FFT Based on OpenMP

Firstly, the acceleration effect of this method is tested by a single machine and multiple threads. The matrices with different data sizes are divided into 2×2, 2×4, and 4×4 blocks, respectively, and each sub-matrix is divided into different threads by OpenMP for independent FFT parallel calculation. Finally, phase compensation was performed.

The numerical results show that the more the blocks are, the higher the acceleration ratio is; the highest acceleration ratio can reach 7.31, but the parallel efficiency shows a downward trend. The highest parallel efficiency of 2×2 blocks can reach 91.5%, and the highest parallel efficiency of 4×4 blocks is 45.7%. The block FFT method in this paper divides the matrix in parallel, and its copy overhead is also allocated in parallel, which significantly improves the parallel efficiency and acceleration ratio compared with the standard FFTW-3.3.5 library (calling 16 threads). Moreover, the acceleration ratio of this method gradually increases with the increase of data scale, and the more the blocks are, the more obvious the growth trend is, which can realize the fast parallel calculation of the FFT algorithm.

At the same time, in Figure 5, the acceleration ratio increases sharply at the scale of 5×10^7. The main reason is that it triggers the bottleneck of memory read speed, which leads to the sharp increase of serial FFT calculation time, but parallel FFT does not trigger the bottleneck of memory read speed, which leads to the sharp increase of acceleration ratio. With the increasing scale, the memory bottleneck gradually weakens, and the acceleration ratio gradually increases after decreasing.

4.2. MPI Parallel Performance of Sea Surface Electromagnetic Scattering Computation Based on FFT Block Method

This section uses a conical wave with an incidence angle of θ and an azimuth angle of $0°$ as the incident source; the tapered wave factor is taken as $L_x/4$, and L_x is the sea surface width. The mesh density is divided into $\lambda/6$ and electromagnetic scattering on the sea surface of the PM/EL sea spectrum with a dielectric constant of $(71.0835, -21.3089)$ by second-order SSA calculation.

Figures 6–7 present the bistatic NRCS for 50 realizations of $10 \times 10\,\mathrm{m}^2$ random sea surfaces generated with the PM and EL spectra, plotted versus incidence angle θ, frequency f, and wind speed U. Figure 8 gives the backscattered NRCS for 50 such realizations obtained with the PM spectrum at 4 GHz and a wind speed of 6.5 m/s. The parallel and serial computations are indistinguishable, confirming that the parallel algorithm preserves accuracy.

Table 1 shows the acceleration ratio and parallel efficiency of sea surface generation at different frequencies when using FFT technology on a $40 \times 40\,\mathrm{m}^2$ sea surface utilization block and calling MPI at four nodes. The results indicate that the larger the computational load is, the higher the sea surface generation efficiency is. At a frequency of 12 GHz, the parallel efficiency of sea surface generation can reach 61.2%, thereby accelerating sea surface generation.

Table 2 shows the calculation of two full-polarization bistatic NRCS acceleration ratios and parallel efficiencies under two $40 \times 40\,\mathrm{m}^2$ sea surfaces using 4-node calling MPI for block FFT acceleration and without calling OpenMP. Multi-scale results analysis is carried out by setting different frequencies to adjust the sea surface mesh density. The results show that the acceleration ratio and parallel efficiency gradually increase with the

TABLE 1. Sea surface parallel generation performance table.

Frequency (GHz)	Serial time (s)	Parallel time (s)	Acceleration ratio	Parallel efficiency (%)
4	8.03	3.79	2.12	52.9
8	35.81	15.13	2.37	59.2
12	79.12	32.34	2.45	61.2

TABLE 2. Comparison of serial and parallel performance of sea surface generation and electromagnetic scattering calculation based on MPI.

Frequency (GHz)	Serial time (s)	Parallel time (s)	Acceleration ratio	Parallel efficiency (%)
4	40232	13513.7	2.98	74.4
8	168166	53914.8	3.12	78.0
12	374268	115917.2	3.23	80.7

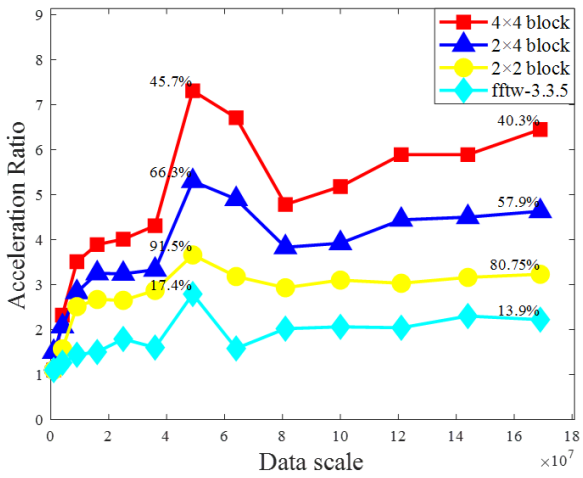

FIGURE 5. Trend chart of parallel acceleration ratio for two-dimensional FFT chunking.

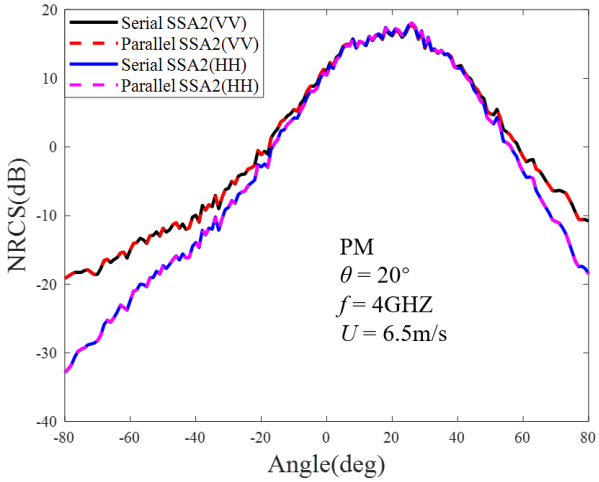

FIGURE 6. Comparison of serial-parallel bistatic NRCS with different polarizations on the Pierson-Moskowitz spectrum (PM) sea surface.

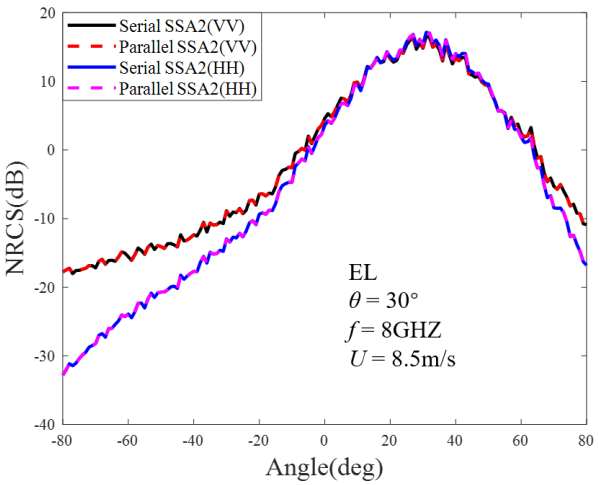

FIGURE 7. Comparison of serial-parallel bistatic NRCS with different polarizations on the Elfouhaily spectrum (EL) sea surface.

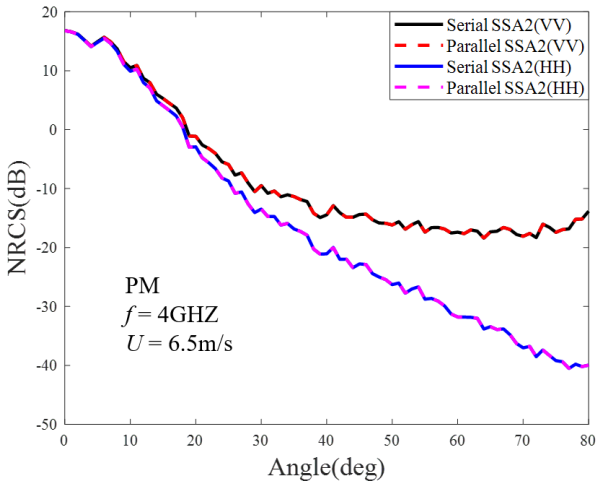

FIGURE 8. Comparison of serial-parallel backscatter NRCS under different polarizations of PM sea surface.

increase in the amount of computation. At 12 GHz, the parallel efficiency reaches 80.7%.

Table 3 shows the use of 4-node calling MPI for block FFT acceleration, calling OpenMP to calculate the full-polarization bistatic NRCS acceleration ratio, and parallel efficiency under two $40 \times 40\,\mathrm{m}^2$ sea surfaces. Multi-scale results analysis is carried out by setting different frequencies to adjust the sea surface mesh density. The results show that the acceleration ratio

TABLE 3. Comparison of serial and parallel performance of sea surface generation and electromagnetic scattering calculation based on MPI + OpenMP.

Frequency (GHz)	Serial time (s)	Parallel time (s)	Acceleration ratio
4	40232	6377.43	6.31
8	168166	25471.3	6.60
12	374268	55091.9	6.79

and parallel efficiency gradually increase with the increase in the amount of computation. At 12 GHz, the acceleration ratio reaches 6.79, which can effectively improve the computational performance of second-order SSA.

5. CONCLUSION

In this paper, a block FFT splitting method for time-varying sea surface generation and parallel calculation of sea surface electromagnetic scattering is proposed. The method splits the data into small blocks and uses MPI to distribute them to individual nodes for independent FFT computation, followed by phase compensation. In a single-machine scenario, no communication is required, and the FFT module achieves a maximum acceleration ratio of 7.31. In multi-machine scenarios, this method combines symmetric domain decomposition to enable the rapid generation of large-scale time-varying sea surfaces and parallel electromagnetic scattering calculations, alleviating memory pressure on a single machine. As data scales increase, parallel efficiency also improves progressively. Under conditions of a 12 GHz incident wave, a $40 \times 40\,\mathrm{m}^2$ sea surface, and four nodes, the overall parallel efficiency reaches 80.7%. When being combined with OpenMP acceleration, the acceleration ratio improves to 6.79, effectively enhancing the computational performance and capacity of the second-order SSA method.

REFERENCES

[1] Mainvis, A., V. Fabbro, C. Bourlier, and H.-J. Mametsa, "Spectral decomposition method for large sea surface generation and radar backscatter modeling," *Journal of Geophysical Research: Oceans*, Vol. 124, No. 12, 8505–8521, 2019.

[2] Li, D., Z. Han, Y. Zhang, Y. Huang, W. Ma, Y. Xue, and Z. Zhao, "A fast method for simulating electromagnetic scattering from sea surface," *IEEE Antennas and Wireless Propagation Letters*, Vol. 23, No. 12, 4413–4417, 2024.

[3] Hall, A. R., "Generalized method of moments," in *A Companion to Theoretical Econometrics*, 230–255, Chapter 11, Wiley, 2003.

[4] Teixeira, F. L., C. Sarris, Y. Zhang, D.-Y. Na, J.-P. Berenger, Y. Su, M. Okoniewski, W. C. Chew, V. Backman, and J. J. Simpson, "Finite-Difference Time-Domain methods," *Nature Reviews Methods Primers*, Vol. 3, No. 1, 75, 2023.

[5] Chou, H.-T. and J. T. Johnson, "A novel acceleration algorithm for the computation of scattering from rough surfaces with the forward-backward method," *Radio Science*, Vol. 33, No. 5, 1277–1287, 1998.

[6] Holmes, M. H., *Introduction to Perturbation Methods*, Springer Science & Business Media, 2012.

[7] Thorsos, E. I., "The validity of the Kirchhoff approximation for rough surface scattering using a Gaussian roughness spectrum," *The Journal of the Acoustical Society of America*, Vol. 83, No. 1, 78–92, 1988.

[8] Afifi, S. and R. Dusséaux, "Scattering from 2-D perfect electromagnetic conductor rough surface: Analysis with the small perturbation method and the small-slope approximation," *IEEE Transactions on Antennas and Propagation*, Vol. 66, No. 1, 340–346, 2018.

[9] Thorsos, E. I. and S. L. Broschat, "An investigation of the small slope approximation for scattering from rough surfaces. Part I. Theory," *The Journal of the Acoustical Society of America*, Vol. 97, No. 4, 2082–2093, 1995.

[10] Guérin, C.-A. and J. T. Johnson, "A simplified formulation for rough surface cross-polarized backscattering under the second-order small-slope approximation," *IEEE Transactions on Geoscience and Remote Sensing*, Vol. 53, No. 11, 6308–6314, 2015.

[11] Frigo, M. and S. G. Johnson, "FFTW: Fastest Fourier transform in the west," *Astrophysics Source Code Library*, ascl–1201, 2012.

[12] Wang, E., Q. Zhang, B. Shen, G. Zhang, X. Lu, Q. Wu, and Y. Wang, "Intel math kernel library," in *High-Performance Computing on the Intel® Xeon Phi™*, 167–188, Springer, 2014.

[13] Wang, C., S. Chandrasekaran, and B. Chapman, "cusFFT: A high-performance sparse fast Fourier transform algorithm on GPUs," in *2016 IEEE International Parallel and Distributed Processing Symposium (IPDPS)*, 963–972, Chicago, IL, USA, 2016.

[14] Scarpino, M., *OpenCL in Action: How to Accelerate Graphics and Computations*, Simon and Schuster, 2011.

[15] Koopman, T. and R. H. Bisseling, "Minimizing communication in the multidimensional FFT," *SIAM Journal on Scientific Computing*, Vol. 45, No. 6, C330–C347, 2023.

[16] Cayrols, S., J. Li, G. Bosilca, S. Tomov, A. Ayala, and J. Dongarra, "Mixed precision and approximate 3D FFTs: Speed for accuracy trade-off with GPU-aware MPI and run-time data compression," Tech. Rep., 2022.

[17] Wang, L., L. Guo, and X. Meng, "Research on electromagnetic scattering characteristics of Kelvin wake of ship based on MPI," in *2018 12th International Symposium on Antennas, Propagation and EM Theory (ISAPE)*, 1–4, Hangzhou, China, 2018.

[18] Jiang, W.-Q., M. Zhang, P.-B. Wei, and X.-F. Yuan, "CUDA-based SSA method in application to calculating EM scattering from large two-dimensional rough surface," *IEEE Journal of Selected Topics in Applied Earth Observations and Remote Sensing*, Vol. 7, No. 4, 1372–1382, 2014.

[19] Voronovich, A. G., "The effect of the modulation of Braggscattering in small-slope approximation," *Waves in Random Media*, Vol. 12, No. 3, 341, 2002.

[20] Wang, J. and X. Xu, "A domain decomposition based technique for 2-D sea surface generation," in *2013 6th International Congress on Image and Signal Processing (CISP)*, 809–813, Hangzhou, China, 2013.